Simulation of General Relativistic Shock Wave Interactions
by a
Locally Inertial Godunov Method
featuring
Dynamical Time Dilation

June 17, 2011

Zeke Vogler[1] *Blake Temple*[2]

1 Introduction

Abstract

We introduce the *locally inertial Godunov method with dynamical time dilation*, and use it to simulate a point of GR shock wave interaction starting from an initial data set that meets the Einstein-Euler constraint equations weakly. The forward time simulations, presented here, resolve the secondary wave in the Smoller-Temple shock wave model for an explosion into a static, singular, isothermal sphere. The backward time solutions indicate black hole formation from a smooth solution via collapse associated with an incoming rarefaction wave. A new feature is that spacetime is approximated as locally flat in each grid cell so that Riemann problems and the Godunov method can be implemented. Clocks are then dynamically dilated to simulate effects of spacetime curvature. Prior work of Groah and Temple justifies meeting the Einstein constraint equations for the initial data only at the weak level of Lipshitz continuity in the metric. As far as we know, this is the first definitive numerical analysis of shock wave interaction in general relativity. In a followup paper, Rientjes and Temple will present Rientjes new proof that such points of shock wave interaction represent a new kind of singularity in general relativity, where spacetime is not locally flat.

We summarize the results in the thesis [16] in which Vogler introduces what we term the *locally inertial Godunov method with dynamic time-dilation*, a fractional step method for simulating spherically symmetric shock-wave solutions of the Einstein-Euler equations in Standard Schwarzschild Coordinates (SSC), [2]. The underlying issue is that the gravitational metric appears to be singular at shock waves in SSC coordinates, the coordinates in which the Einstein equations take the simplest form, [2]. The simulations here give a

[1]This work summarizes results that first appeared in Vogler's doctoral dissertation, [16]

[2]Department of Mathematics, University of California, Davis, Davis CA 95616; Supported by NSF Applied Mathematics Grant Number DMS-070-7532

definitive numerical demonstration that the locally inertial Godunov method is nevertheless a viable first order numerical method for simulating shock waves in SSC. Numerical convergence of the method is demonstrated for an initial data set obtained by matching a critically expanding Friedmann-Robertson-Walker (FRW) spacetime to the inside of a static Tolmann-Oppenheimer-Volkoff (TOV) solution, creating a point of shock wave interaction.[3] The subsequent evolution provides a simple model for a general relativistic (GR) explosion containing both an imploding and exploding shock wave. The backward time evolution shows black hole formation from an imploding expansion wave. The theory in [2] confirms that the FRW and TOV solutions need only join up Lipschitz continuously at fixed time in order to meet the Einstein constraint equations weakly. The most interesting new feature of the numerical method is that curved spacetime is approximated by Minkowski flat spacetime in each grid cell making approximation by Riemann problems (RP) and the Godunov method viable, and this is compensated for by dilating the clocks in each grid cell to account for spacetime curvature. In this paper we record the elements of the numerical method at a level sufficient for replication, present a definitive case for convergence of the method, and establish the Lipschitz structure of the gravitational metric at points of shock wave interaction in the forward time simulation of a GR explosion. In a followup paper, Rientjes and Temple will present Rientjes' new proof [4] that at such points of shock wave interaction, the gravitational metric is essentially only Lipschitz continuous, cannot be smoothed by coordinate transformation, and as a consequence, points of shock wave interaction simulated here represent a new kind of singularity in general relativity, where spacetime is not locally flat.

The point of departure for this work is the existence theory [2], in which Groah and second author prove existence of weak shock wave solutions of the Einstein equations in SSC for gravitational metrics that are only $C^{0,1}$ (Lipschitz continuous)[5] at shock waves. Weak solutions are proven to exist for finite time starting from an initial $C^{0,1}$ gravitational metric, and initial density and velocity profiles of bounded total variation. Although solutions appear to be singular at shocks in the sense that second derivatives of the $C^{0,1}$ gravitational metrics contain delta function sources, the analysis shows that the delta functions cancel out in the curvature tensor, and the Einstein equations are satisfied weakly. This analysis was the first to connect general relativity to the Glimm scheme through a locally inertial formulation of the Einstein-Euler equations. The locally inertial formulation is amenable to approximation locally by flat Minkowski spacetime, so exact RP solutions for the relativisitic compressible Euler equations can be used in each grid cell, thereby making the analysis of a fractional step Glimm scheme feasible, [4, 1, 8]. Although the conclusion is that solutions with Lipschitz continuous gravitational metrics make physical sense in SSC as weak solutions of the Einstein equations in the presence of arbitrary numbers of interacting shock waves of arbitrary strength, [2] is a general theorem, and there is no known analysis that rigorously details the local structure of solutions at shock wave interactions. In his thesis [16], Vogler developed these ideas into a viable numerical method, and used it to carefully simulated a point of GR

[3]Shock surfaces generically intersect on a two dimensional surface in spacetime, but radial shocks with spherical symmetry intersect on a three dimensional surface, and cross at a single point in the (t, r) plane.

[4]The problem was first proposed in second author's NSF grant DMS-070-7532.

[5]Here, $C^{k,l}$ denotes the space of k-continuously differentiable functions whose kth derivative is Holder continuous with exponent l, $C^{0,1}$ then denoting the space of Lipschitz continuous functions, c.f. [2].

shock wave interaction in forward time, and black hole formation in backward time. This is interesting from several standpoints.

First, the numerics and supporting analysis establish and clarify the $C^{0,1}$ structure of the gravitational metric at points of shock wave interaction. This sets the stage for the forthcoming paper with Reintjes which supplies a proof that, in contrast to Israel's Theorem for single shock surfaces [5], (which states that the gravitational metric can always we smoothed from $C^{0,1}$ to $C^{1,1}$ at points on a smooth shock surface in GR), gravitational metrics with this structure cannot be smoothed to $C^{1,1}$ by coordinate transformation, the level of smoothness usually assumed in GR, [10, 3]. In particular, taken together, this demonstrates that there do not exist coordinate systems better than SSC in which the weak solutions constructed by Groah and Temple are actually $C^{1,1}$ strong solutions of the Einstein equations when shock wave interactions are present.

Another point of interest is that we can assume the fundamental equation of state $p = \sigma\rho$, $\sigma = c^2/3$,[6] and thereby dovetail nicely with the results in [9] which established that this is a relativistic Nishida system for flat Minkowski spacetime. We employ the exact global solution of the RP of [9], greatly simplifying the RP step of the locally inertial Godunov method, [9, 14], c.f. [7, 9].

The initial data set is also interesting in its own right as a natural starting point for a rigorous proof of GR shock-wave or black hole formation from smooth solutions. It is constructed by matching initial data from a critical ($k = 0$) FRW spacetime in self-similar coordinates [15], to initial data for the exact TOV solution modeling a general relativistic static singular isothermal sphere [11], and there is a one parameter family of such matchings. The forward time simulation can be interpreted as resolving the secondary reflected wave in the Smoller-Temple model of a GR explosion into a static isothermal sphere [11]. The original Smoller-Temple model was the first example of an exact GR shock wave, and exact formulas were obtained by eliminating the secondary (incoming) reflected wave, this being effected by a change in equation of state across the outgoing shock, (approximating a drop in in temperature across the shock in the isothermal case $\sigma < c^2/3$). Assuming no change in the equation of state at the shock, correct when $\sigma = c^2/3$, the numerics demonstrate that the secondary reflected wave is an incoming shock wave, not a rarefaction wave. And finally, because the initial data set agrees with exact solutions on either side of the FRW-TOV intersection, finite speed of propagation implies that exact boundary conditions can be imposed and convergence can be tested on either side of a bounded region of interaction. In particular, the method entails starting with boundary data on the FRW side of the simulation, and integrating through the region of interaction to recover (up to transformation of the SSC time variable) the TOV metric on the other side. Thus we have a GR framework tailored for a definitive test of convergence of numerical methods at shock waves.

We note also that because the existence theory in [2] applies when the gravitational metric

[6]Here p is the pressure, ρ is the energy density, c is the speed of light, and $p = \frac{c^2}{3}\rho$ is the exact equation of state for both pure radiation and the extreme relativisitc limit of free particles, c.f. [17].

is only $C^{0,1}$, the Einstein equations are satisfied only weakly in the sense of the theory of distributions, at shock waves. For the Einstein equations to hold strongly, the metric must be at least $C^{1,1}$, one degree smoother. But the admissibility of metrics at the lower regularity $C^{0,1}$ in SSC is what makes it feasible to create viable initial data from exact FRW and TOV solutions because, to meet the Einstein constraint equations weakly on the initial data set in SSC, solutions need only match Lipschitz continuously at a given time. Matching metrics at the stronger level of $C^{1,1}$ would be problematic.

The numerical demonstrations are backed up by Theorem 9.1 below, which states that if a sequence of approximate solutions generated by the locally inertial Godunov method converge pointwise almost everywhere and the total variation of the fluid variables remains uniformly bounded in time, then the limit solution is an exact weak solution to the Einstein equations. By this general theorem it suffices only to demonstrate numerical convergence to a limit, with bounded oscillations, in order to conclude the simulated solutions accurately represent exact (weak) solutions of the Einstein equations.

For the backward time solution in [16], the simulation shows black hole formation via collapse by an incoming expansion wave, (a generalized rarefaction wave). Since black holes cannot form in finite time in SSC due to infinite time-dilation at the Schwarzschild radius, we argue for black hole formation by numerically confirming the solution gets well within the Buchdahl stability limit of 9/8 the Schwarzschild radius, the limit beyond which there exists no static configuration sufficient to hold the mass up from the inside, [12]. Specifically, we take the numerics to a time-dilation factor of 2.9×10^4, and black hole number $2\mathcal{G}M/r = .922 \geq .888...$, the latter being the Buchdahl limit. This calculation took about a week to perform on a PC. A proposal for future research is to simulate all the way into and through the black hole by continuing the evolution via a locally inertial formulation of the equations in transformed coordinates, like Eddington-Finkelstein or Kruskal, that regularize the singularity at the Schwarzschild radius, [17]. (See [6] and references therein for a numerical investigation of black hole and shock wave formation by shock capturing methods.)

In Section 2 we introduce the Einstein-Euler equations, and the FRW and TOV exact solutions. In Section 3 we give formulas for the FRW metric in SSC coordinates. In Section 4 we give formulas for a TOV static isothermal sphere. In 5 we give one parameter family of matched FRW-TOV initial data. In 6 we give the elements of the locally inertial Godunov method. In Section 7 we discuss the Riemann problem step of the method. In Section 8 we put in the time-dilation. In Section 9 we state Theorem 9.1 on convergence. In Section 10 we present the forward time simulations, and give a definitive numerical demonstration of the convergence of the locally inertial Godunov method in the presence of shock waves. Section 10 we put in dimensions to give an indication of the physical regimes to which the simulations apply.

2 Preliminaries

The Einstein-Euler equations

$$G = \kappa T, \tag{1}$$

of general relativity are equations for the gravitational metric tensor g, coupled to the relativistic compressible Euler equations through the identity

$$Div\ T = 0. \tag{2}$$

Here G is the Einstein curvature tensor, T is stress energy tensor for a perfect fluid, and κ is the coupling constant

$$\kappa = \frac{8\pi\mathcal{G}}{c^4}, \tag{3}$$

where $\mathcal{G}$ is Newton's gravitational constant, and we use the convention that $c = 1$ and $\mathcal{G} = 1$ whenever convenient, [17]. In component form,

$$G^{ij} = \kappa T^{ij}, \tag{4}$$

$$T^{ij} = (\rho + p)w^i w^j + pg^{ij}, \tag{5}$$

and

$$ds^2 = g_{ij}dx^i dx^j,$$

where $\mathbf{w} = (w^0, ..., w^3)$ is the unit 4-velocity, ρ the energy density, p the pressure, and we use the Einstein summation convention whereby indices $i, j = 0, ..., 3$ are raised and lowered with the metric, and summation is assumed on repeated up-down indices.

We restrict to spherically symmetric gravitational metrics in SSC coordinates

$$ds^2 = -B(t, r)dt^2 + \frac{1}{A(t, r)}dr^2 + r^2 d\Omega^2, \tag{6}$$

$$A(t, r) = 1 - \frac{2\mathcal{G}M}{r}, \tag{7}$$

where M is the mass fuction, (t, r) are temporal and radial coordinates, $d\Omega^2 = d\theta^2 + \sin^2\theta d\phi^2$ represents the standard line element of the unit 2-sphere, and $x \equiv (x^0, \ldots, x^3) \equiv (t, r, \theta, \phi)$ is the spacetime coordinate system. It is well known that a general spherically symmetric gravitational metric of form

$$ds^2 = -A(t, r)dt^2 + B(t, r)dr^2 + 2D(t, r)dtdr + C(t, r)d\Omega^2, \tag{8}$$

can, under generic conditions, be transformed over to SSC, [17].

Putting the SSC metric ansatz (6) into MAPLE, (suppressing the bars), the Einstein equations $G = \kappa T$ reduce to the four partial differential equations[7]

$$\left\{-r\frac{A_r}{A} + \frac{1-A}{A}\right\} = \frac{\kappa B}{A} r^2 T^{00} \tag{9}$$

$$\frac{A_t}{A} = \frac{\kappa B}{A} r T^{01} \tag{10}$$

$$\left\{r\frac{B_r}{B} - \frac{1-A}{A}\right\} = \frac{\kappa}{A^2} r^2 T^{11} \tag{11}$$

$$-\left\{\left(\frac{1}{A}\right)_{tt} - B_{rr} + \Phi\right\} = 2\frac{\kappa B}{A} r^2 T^{22}, \tag{12}$$

where

$$\Phi = \frac{B_t A_t}{2A^2 B} - \frac{1}{2A}\left(\frac{A_t}{A}\right)^2 - \frac{B_r}{r} - \frac{BA_r}{rA} + \frac{B}{2}\left(\frac{B_r}{B}\right)^2 - \frac{B}{2}\frac{B_r}{B}\frac{A_r}{A},$$

and subscripts denote partial differentiation.

In the presence of shock waves, the stress-energy tensor T is discontinuous, and thus A and B in (9)-(12) are Lipschitz continuous at best. In this case equation (12), is satisfied only in the weak sense. In [14] it is shown that when the metric is Lipschitz and and the stress-energy tensor is bounded in sup-norm, system (9)-(12) is weakly equivalent to the system obtained by replacing (10) and (12) with $\nabla_i T^{i0} = 0$ and $\nabla_i T^{i1} = 0$, respectively, (c.f. (2)), and these can be written in the *locally inertial* form

$$\{T_M^{00}\}_{,0} + \left\{\sqrt{AB}T_M^{01}\right\}_{,1} = -\frac{2}{x}\sqrt{AB}T_M^{01}, \tag{13}$$

$$\{T_M^{01}\}_{,0} + \left\{\sqrt{AB}T_M^{11}\right\}_{,1} = -\frac{1}{2}\sqrt{AB}\left\{\frac{4}{x}T_M^{11} + \frac{(\frac{1}{A}-1)}{x}(T_M^{00} - T_M^{11}) + \frac{2\kappa x}{A}(T_M^{00}T_M^{11} - (T_M^{01})^2) - 4xT^{22}\right\}, \tag{14}$$

where T_M^{ij}, are the Minkowski stresses, related to T^{ij} by

$$T_M^{00} = BT^{00}, \tag{15}$$

$$T_M^{01} = \sqrt{\frac{B}{A}}T^{01}, \tag{16}$$

$$T_M^{11} = \frac{1}{A}T^{11}, \tag{17}$$

[7]Beware that in [2], A is used for the dt^2 coefficient and B for the dr^2 coefficient of the metric.

and

$$T^{22} = \frac{\sigma\rho}{x^2}. \tag{18}$$

Here, $\{\}_{,0}$ and $\{\}_{,1}$ denote derivatives with respect to t and r, respectively. The remaining two equations (9) and (11) can then be rearranged as

$$\frac{A'}{A} = \frac{(\frac{1}{A}-1)}{x} - \frac{\kappa x}{A}T_M^{00}, \tag{19}$$

$$\frac{B'}{B} = \frac{(\frac{1}{A}-1)}{x} + \frac{\kappa x}{A}T_M^{11}. \tag{20}$$

We use the following formula for the M obtained from (7) and (15),

$$M(t,r) = M(t,r_0) + \frac{\kappa}{2}\int_{r_0}^{r} T_M^{00}(t,r)r^2 dr. \tag{21}$$

When $\sigma = const.$ and

$$p = \sigma\rho, \tag{22}$$

the components of T_M are given by

$$T_M^{00} = \frac{c^4 + \sigma^2 v^2}{c^2 - v^2}\rho, \tag{23}$$

$$T_M^{01} = \frac{c^2 + \sigma^2}{c^2 - v^2}cv\rho, \tag{24}$$

$$T_M^{11} = \frac{v^2 + \sigma^2}{c^2 - v^2}c^2\rho, \tag{25}$$

where v is the velocity.

$$v = \frac{1}{\sqrt{AB}}\frac{u^1}{u^0},$$

c.f. [2]. The main point is that T_M is independent of the metric, and unlike T, the equations (15)-(20) close when T_M^{0j} are taken as the conserved quantities.

Using x in place of r, the equations take the form of a system of conservation laws with sources,

$$\begin{aligned} u_t + f(\mathbf{A}, u)_x &= g(\mathbf{A}, u, x), \\ \mathbf{A}' &= h(\mathbf{h}, u, x), \end{aligned} \tag{26}$$

where

$$u = (T_M^{00}, T_M^{01}) \equiv (u^0, u^1) \tag{27}$$

are the Minkowski energy and momentum densities,

$$\mathbf{A} = (A, B) \tag{28}$$

are the metric components,

$$f(\mathbf{A}, u) = \sqrt{AB}\ (T_M^{01}, T_M^{11}) \tag{29}$$

is the flux,

$$g(\mathbf{A}, u, x) = (g^0(\mathbf{A}, u, x), g^1(\mathbf{A}, u, x)),$$

with

$$g^0(\mathbf{A}, u, x) = -\frac{2}{x}\sqrt{AB}T_M^{01}, \tag{30}$$

$$g^1(\mathbf{A}, u, x) = -\frac{1}{2}\sqrt{AB}\left\{\frac{4}{x}T_M^{11} + \frac{(\frac{1}{A} - 1)}{x}(T_M^{00} - T_M^{11}) + \frac{2\kappa x}{A}(T_M^{00}T_M^{11} - (T_M^{01})^2) - 4xT^{22}\right\}, \tag{31}$$

gives the source term of the balance law, and

$$h(\mathbf{A}, u, x) = (h^0(\mathbf{A}, u, x), h^1(\mathbf{A}, u, x)), \tag{32}$$

with

$$h^0(\mathbf{A}, u, x) = \frac{(1 - A)}{x} - \kappa x T_M^{00}, \tag{33}$$

$$h^1(\mathbf{A}, u, x) = \frac{B}{A}\left\{\frac{(1 - A)}{x} + \kappa x T_M^{11}\right\}, \tag{34}$$

is the source term for the metric.

Our purpose is to introduce an effective first order method, the locally inertial Godunov method, and use it to compute a family of weak solutions of system (26).

3 Exact FRW Solutions in SSC

The Einstein equations for the $k = 0$ FRW metric

$$ds^2 = -dt^2 + R^2(t)\{dr^2 + r^2 d\Omega^2\}, \tag{35}$$

in co-moving coordinates are

$$H^2 = \tfrac{\kappa}{3}\rho - k, \tag{36}$$

$$\dot{\rho} = -3(\rho + p)H. \tag{37}$$

When $p = \rho c^2/3$, the solution is

$$\rho(t) = \frac{3}{4\kappa t^2}, \tag{38}$$

where we have assumed t is time since the big bang, [15].

To match FRW to TOV in SSC, we use the following representation of FRW found in [15].

Theorem 3.1. *Assume $p = \frac{1}{3}\rho$ and $k = 0$. Then the FRW metric (35) under the coordinate transformation*

$$\begin{aligned} \bar{r} =& \sqrt{t} r, \\ \bar{t} =& \left\{ 1 + \frac{\bar{r}^2}{4t^2} \right\} t = t + \frac{r^2}{4}, \end{aligned} \tag{39}$$

goes over to the following metric in SSC

$$ds^2 = -\frac{1}{1-v^2} d\bar{t}^2 + \frac{1}{1-v^2} d\bar{r}^2 + \bar{r}^2 d\Omega^2, \tag{40}$$

where the fluid velocity v is related to $\bar{r}/\bar{t}$ by

$$\xi \equiv \frac{\bar{r}}{\bar{t}} = \frac{2v}{1+v^2}. \tag{41}$$

A direct consequence is the following Corollary.

Corollary 3.1. *The fluid variables (ρ, v) corresponding to (40) satisfy*

$$\rho(\xi, \bar{r}) = \frac{3v(\xi)^2}{\kappa \bar{r}^2}, \qquad v(\xi) = \frac{1 - \sqrt{1-\xi^2}}{\xi}. \tag{42}$$

4 Exact TOV Solutions in SSC

The general relativistic version of TOV metrics that model static singular isothermal spheres was described in [9]. Assuming $p = \sigma\rho$, these are given by

$$ds^2 = -B(\bar{r}) d\bar{t}^2 + \left(\frac{1}{1 - \frac{2\mathcal{G}M(\bar{r})}{\bar{r}}} \right) d\bar{r}^2 + \bar{r}^2 d\Omega^2, \tag{43}$$

with

$$\begin{aligned} B(\bar{r}) &= B^t(\bar{t}) B_0(\bar{r})^{\frac{4\sigma}{1+\sigma}}, && (44) \\ A(\bar{r}) &= 1 - 8\pi\mathcal{G}\gamma, && (45) \\ M(\bar{r}) &= 4\pi\gamma\bar{r}, && (46) \end{aligned}$$

and

$$\rho(\bar{r}) = \frac{\gamma}{\bar{r}^2}, \qquad v = 0, \tag{47}$$

where

$$\gamma = \frac{1}{2\pi\mathcal{G}} \left(\frac{\sigma}{1 + 6\sigma + \sigma^2} \right), \tag{48}$$

depends on σ. The velocity is zero because the TOV metric is a time independent metric in SSC coordinates, (c.f. equation (3.4) of [10]). The arbitrary function $B^t(\bar{t})$ is included to account for the time scale freedom in (43), a freedom required to match the simulated FRW-TOV solution at a later time. That is, our simulation involves integrating the metric starting from FRW boundary data on the left hand side of the simulation, and the TOV metric comes out of the simulation to the right of a region of interaction. But the time-scaling function $B^t(\bar{t})$ comes out of the simulation, cannot be imposed ahead of time, and as a result, the TOV metric must be re-matched by adjusting $B^t(\bar{t})$ at each time step.

5 One Parameter Family of Shock Wave Initial Data

Assume an initial time $\bar{t}_0 > 0$ and radius $\bar{r}_0$ to be determined later. We match the metric components (A, B) of the FRW and TOV metrics (35) and (43) Lipschitz continuously at $(\bar{t}_0, \bar{r}_0)$, thereby posing an initial discontinuity in the fluid variables. By (40) and (45) we have

$$A_{FRW}(\bar{t}_0, \bar{r}_0) = 1 - v \left(\frac{\bar{r}_0}{\bar{t}_0} \right)^2 = 1 - 8\pi\mathcal{G}\gamma = A_{TOV}(\bar{t}_0, \bar{r}_0). \tag{49}$$

Let $v_0 = v(\bar{r}_0/\bar{t}_0)$ represent the fluid velocity on the FRW side of the discontinuity so (49) implies

$$v_0 = \sqrt{8\pi\mathcal{G}\gamma} = \sqrt{\frac{4\sigma}{1 + 6\sigma + \sigma^2}}. \tag{50}$$

Note that v_0 is independent of the the free parameter r_0. Using (41) we find the unknown starting time $\bar{t}_0$ as

$$\bar{t}_0 = \frac{\bar{r}_0(1 + v_0^2)}{2v_0}. \tag{51}$$

The independence of v_0 from $\bar{r}_0$ along with (51) implies the initial start time is proportional to the initial radius of the discontinuity. Finding $\bar{t}_0$ enables us to build the initial profile of the FRW metric for any radial coordinate $\bar{r} < \bar{r}_0$ by computing $\xi = \bar{r}/\bar{t}_0$ and using equations (40)-(42).

On the TOV side, A is already determined as the constant (45). To find B, use (40) and (44) to get

$$B_{TOV}(\bar{t}_0, \bar{r}_0) = B_0(\bar{r}_0)^{\frac{4\sigma}{1+\sigma}} = \frac{1}{1 - v_0^2} = B_{FRW}(\bar{t}_0, \bar{r}_0), \tag{52}$$

forcing the constant B_0 to take the form

$$B_0 = \frac{\bar{r}_0^{-\frac{4\sigma}{1+\sigma}}}{1 - v_0^2}. \tag{53}$$

Combining (49)-(53) in the case $\sigma = 1/3$, and letting $\xi = \bar{r}/\bar{t}_0$, we define the initial data $v_{init}(\bar{r})$, $\rho_{init}(\bar{r})$, $A_{init}(\bar{r})$, and $B_{init}(\bar{r})$ posed at time $\bar{t}_0$, depending on the free parameter $\bar{r}_0$, as follows.

$$v_{init}(\bar{r}) = \begin{cases} \frac{1-\sqrt{1-\xi^2}}{\xi} & \bar{r} < \bar{r}_0 \\ 0 & \bar{r} > \bar{r}_0, \end{cases} \tag{54}$$

$$\rho_{init}(\bar{r}) = \begin{cases} \frac{3v_{init}^2}{\kappa \bar{r}^2} & \bar{r} < \bar{r}_0 \\ \frac{\gamma}{\bar{r}^2} & \bar{r} > \bar{r}_0, \end{cases} \tag{55}$$

$$A_{init}(\bar{r}) = \begin{cases} 1 - v_{init}^2 & \bar{r} < \bar{r}_0 \\ 1 - 8\pi\mathcal{G}\gamma & \bar{r} > \bar{r}_0, \end{cases} \tag{56}$$

and

$$B_{init}(\bar{r}) = \begin{cases} \frac{1}{1-v_{init}^2} & \bar{r} < \bar{r}_0 \\ B_0(\bar{r})^{\frac{4\sigma}{1+\sigma}} & \bar{r} > \bar{r}_0. \end{cases} \tag{57}$$

6 Locally Inertial Godunov Method

In this section we define the algorithm for the locally inertial Godunov method.

To start, fix a minimum radius r_{min}, a maximum radius r_{max}, the number of spatial gridpoints n, and a start time t_0. In our simulations, the number of spatial grid points n is chosen to be a power of two (i.e. $n = 2^k$ for some k). From these parameters, the mesh width Δx is determined to be

$$\Delta x = \frac{r_{max} - r_{min}}{n - 1}, \tag{58}$$

and is fixed throughout the scheme. Let (x_i, t_j) represent a mesh point in an unstaggered grid defined on the domain

$$D = \{r_{min} \leq x_i \leq r_{max}, t_j \geq t_0\}. \tag{59}$$

The spatial points are defined as

$$x_i \equiv r_{min} + (i-1)\Delta x \text{ for } i = 1, \ldots, n. \tag{60}$$

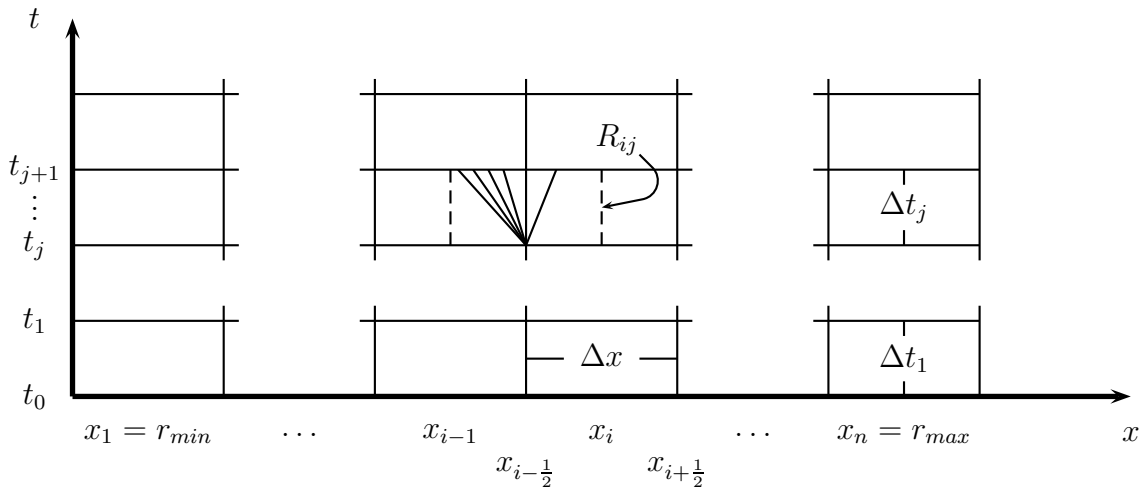

Figure 1: The Riemann cell R_{ij}

Unlike the mesh width, the time step or the mesh height, Δt, changes from one time step to the next because there is no way to determine beforehand the smallest Δt satisfying the CFL condition for every time step. So for every time t_j, a new time step is computed by

$$\Delta t_j = \min\left\{\frac{\Delta x}{2\sqrt{A_{ij}B_{ij}}}\right\}, \tag{61}$$

where the minimum is taken over all the spatial gridpoints at time t_j of the metric $\mathbf{A}_{ij} = (A_{ij}, B_{ij})$, to be defined shortly. Starting at t_0, the temporal mesh points are defined by

$$t_j \equiv t_0 + \sum_{k=1}^{j} \Delta t_k \text{ for } j = 1, \ldots, \infty. \tag{62}$$

We assume at our current time t_j for $j \geq 0$ there exists a solution $u(t_j, x)$ and $\mathbf{A}(t_j, x)$ for $(t_j, x) \in D$. This solution is either provided as the starting solution at t_0 or from the last iteration of the locally inertial Godunov scheme constructed inductively. To implement the method, this solution is discretized into piecewise constant states. Discretizing the conserved quantities $u(t_j, x)$, let $u_{\Delta x}$ be given by piecewise constant states u_{ij} at time $t = t_j^+$ as follows:

$$u_{\Delta x}(t, x) = u_{ij} \equiv u(t_j, x_i) \text{ for } x_{i-} \leq x < x_{i+}, t = t_j^+. \tag{63}$$

For notational convenience, we denote $x_{i+} \equiv x_{i+\frac{1}{2}}$ and $x_{i-} \equiv x_{i-\frac{1}{2}}$ throughout this paper.

We define the grid rectangle R_{ij} so the mesh point (x_{i-}, t_j) is in the bottom center of it,

$$R_{ij} \equiv \{x_{i-1} \leq x < x_i,\ \ t_j \leq t < t_{j+1}\}, \qquad 1 \leq i \leq n+1,\ \ j \geq 0, \tag{64}$$

which is diagrammed in Figure 1. Each grid rectangle is a Riemann cell, containing a solution to a distinct Riemann problem. We are limited to solving Riemann problems within Riemann

cells having a constant speed of light. To this end, the metric source $\mathbf{A} = (A, B)$ must be approximated by a constant value, denoted $\mathbf{A}_{ij}$, in each Riemann cell R_{ij} throughout the simulation. These constant values are established by setting

$$\mathbf{A}_{\Delta x}(t, x) = \mathbf{A}_{ij} \equiv \mathbf{A}(t_j, x_{i-}) \text{ for } (t, x) \in R_{ij}. \tag{65}$$

This approximation makes $\mathbf{A}_{\Delta x}$ discontinuous along each line $x = x_i, i = 1, \ldots, n$, at each time step $t = t_j$.

To implement the Godunov step, we need boundary profiles at the left and right boundaries along with the initial profiles at time t_0 because the Godunov step is a three point method, and the points x_1 and x_n need left and right partners, respectively, to pose the boundary Riemann problems. These boundary profiles are used to implement the boundary Riemann problems and are referred to as *ghost cells*. The left and right ghost cells, located at the points x_0 and x_{n+1}, respectively, must be consistent with our numerical solution to the Einstein equations around these boundaries. Any inconsistency in these boundary conditions would result in errors propagating into the solution, corrupting the data; therefore, data is needed for the left ghost cell $u_{0,j}$ and $\mathbf{A}_{0,j}$ along with the right ghost cell $u_{n+1,j}$ and $\mathbf{A}_{n+1,j}$ that are solutions to the Einstein equations synchronized with the data close to the boundary. Figure 2 displays the location of these ghost cells.

For the ghost cell on the FRW side at the gridpoint x_0, use (42) to express the fluid velocity as a function of time $\bar{t}_j$

$$v_{0,j} = \frac{1 - \sqrt{1 - \xi^2}}{\xi}, \tag{66}$$

where $\xi = x_0/\bar{t}_j$. With this fluid velocity, the fluid density becomes

$$\rho_{0,j} = \frac{3v_{0j}^2}{\kappa x_0^2}. \tag{67}$$

Since the metric components are staggered relative to the fluid variables, we need to compute the half gridpoint

$$x_{\frac{1}{2}} = x_0 + \frac{\Delta x}{2}, \tag{68}$$

and use it to find the corresponding velocity

$$v_{\frac{1}{2},j} = \frac{1 - \sqrt{1 - \xi^2}}{\xi}, \tag{69}$$

for $\xi = x_{\frac{1}{2}}/\bar{t}_j$. We use this velocity to compute the metric components,

$$A_{1,j} = 1 - v_{\frac{1}{2},j}^2, \qquad B_{1j} = \frac{1}{1 - v_{\frac{1}{2},j}^2}. \tag{70}$$

The boundary condition for the TOV is static, so values of the fluid variables and the metric component A are constant in time, but the function B changes by the time scale factor B^t in

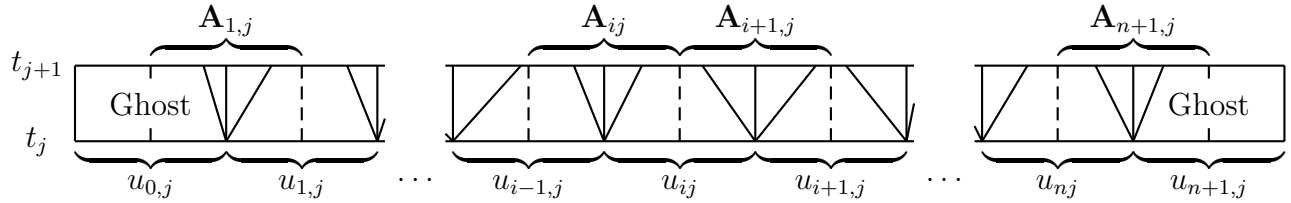

Figure 2: Staggering of the metric $\mathbf{A}$ and the solution u

(44), and must be rematched during each time step, as discussed in the last section. Using the above criteria for the TOV ghost cell, let x_n be the gridpoint position of this border. We rematch the time scale at time $\bar{t}_j$ by the following formula

$$B^t = B(\bar{t}_j, x_n)(x_n)^{-\frac{4\sigma}{1+\sigma}}, \tag{71}$$

where $B(\bar{t}_j, x_n)$ is the simulated solution at the coordinate $(\bar{t}_j, x_n)$.

The discontinuities of the metric $\mathbf{A}_{\Delta x}$ are staggered relative to the approximate solution $u_{\Delta x}$ as illustrated in Figure 2. This staggering puts constant metric values within each Riemann cell and constant conserved quantity states at the bottom of each Godunov cell. Constant conserved quantities $u_{\Delta x}$ in each Godunov cell and a constant metric $\mathbf{A}_{\Delta x}$ in each Riemann cell enables us to pose Riemann problems in locally inertial coordinate frames where we are capable of solving the relativistic compressible Euler equations. More specifically, there is a Riemann problem at the bottom center of each Riemann cell R_{ij}

$$\begin{gathered} u_t + f(\mathbf{A}_{ij}, u)_x = 0 \\ u_0(x) = \begin{cases} u_L = u_{i-1,j} & x < x_{i-} \\ u_R = u_{i,j} & x > x_{i-}. \end{cases} \end{gathered} \tag{72}$$

Let $u_{ij}^{RP}(t,x)$ denote the solution of (72) within the Riemann cell R_{ij}, and define

$$u_{\Delta x}^{RP}(t,x) \equiv u_{ij}^{RP}(t,x) \text{ for } (t,x) \in R_{ij} \tag{73}$$

as the Riemann problem step of the fractional step scheme.

Given the solutions to the Riemann problems in each Riemann cell R_{ij}, we implement the Godnunov step to obtain the average of fluid variables $u_{\Delta x}^{RP}$ across the intervals $[x_{i-}, x_{i+}]$ at the next time step t_{j+1}. Since the metric $\mathbf{A}$ is different on both sides of x_i, separate averages must be taken over the left and right half cells and combined to obtain the true average. In particular, let $\bar{u}_{ij}^L$ and $\bar{u}_{ij}^R$ be the average on the left and right half cells, respectively. Also, let $u_*^L = u_{ij}^{RP}(t_{j+1}^-, x_{i-})$ and $u_*^R = u_{ij}^{RP}(t_{j+1}^-, x_{i+})$ represent the zero speed states left and right Riemann problem, respectively, as shown in Figure 2. To perform the Godunov step on the left half cell, we compute

$$\bar{u}_{ij}^L = u_{ij} - \frac{2\Delta t}{\Delta x}\{f(\mathbf{A}_{ij}, u_{ij}) - f(\mathbf{A}_{ij}, u_*^L)\}, \tag{74}$$

and do the same for the right half cell

$$\bar{u}_{ij}^R = u_{ij} - \frac{2\Delta t}{\Delta x}\{f(\mathbf{A}_{ij}, u_*^R) - f(\mathbf{A}_{ij}, u_{ij})\}, \tag{75}$$

where the 2 accounts for the half cell calculations. Taking the average of these results leads to

$$\bar{u}_{ij} = \frac{1}{2}\{\bar{u}^L_{ij} + \bar{u}^R_{ij}\}, \tag{76}$$

defining our Godunov step of the method.

We proceed to define the ODE step. Let $\hat{u}(t, u_0)$ denote the solution to the following initial value problem

$$\begin{gathered} \hat{u}_t = G(\mathbf{A}_{ij}, \hat{u}, x) = g(\mathbf{A}_{ij}, \hat{u}, x) - \mathbf{A}' \cdot \nabla_{\mathbf{A}} f(\mathbf{A}_{ij}, \hat{u}, x), \\ \hat{u}(0) = u_0, \end{gathered} \tag{77}$$

where $G(\mathbf{A}, \hat{u}, x) = (G^0, G^1)$ takes the form

$$G^0 = -\frac{1}{2}\sqrt{AB}\left(\frac{c^2+\sigma^2}{c^2-v^2}\right) cv\frac{\rho}{x}\left\{2(\frac{1}{A}+1) - \frac{\kappa}{A}(c^2-\sigma^2)\rho x^2\right\}, \tag{78}$$

$$G^1 = -\frac{1}{2}\sqrt{AB}\left(\frac{c^2+\sigma^2}{c^2-v^2}\right) \frac{\rho}{x}\left\{4v^2 + (\frac{1}{A}-1)(c^2+v^2) + \frac{\kappa}{A}(\sigma^2-v^2)c^2\rho x^2\right\}. \tag{79}$$

We define the approximate solution $u_{\Delta x}(t, x)$ and $\mathbf{A}_{\Delta x}(t, x)$ analytically to derive the piecewise formulas used to update the numerical scheme and to be used in the convergence proof of Section 9. The conserved quantities are defined by the formula

$$u_{\Delta x}(t, x) = u^{RP}_{\Delta x}(t, x) + \int_{t_j}^{t} \{G(\mathbf{A}_{ij}, \hat{u}(\xi - t_j, u^{RP}_{\Delta x}(t, x), x)\} d\xi \tag{80}$$

Therefore, $u_{\Delta x}(t, x)$ is equal to $u^{RP}_{\Delta x}(t, x)$, the solution to the Riemann problems, plus a correction term from the ODE step of the method. The metric is derived from the definition of the mass

$$M_{\Delta x}(x, t) = M_{r_{min}} + \frac{\kappa}{2}\int_{r_{min}}^{x} u^0_{\Delta x}(r, t) r^2 dr. \tag{81}$$

In terms of these equations, define the metric as

$$A_{\Delta x}(x, t) = 1 - \frac{2M_{\Delta x}(x, t)}{x}, \tag{82}$$

and

$$B_{\Delta x}(x, t) = B_{r_0} \exp \int_{r_{min}}^{x} \left\{\frac{\{A_{\Delta x}(r, t)\}^{-1} - 1}{r} + \frac{\kappa r}{A_{\Delta x}(r, t)} T^{11}_M(u_{\Delta x}(r, t))\right\} dr. \tag{83}$$

Finally, in order to update the metric and conserved quantities, we use the Riemann problem averages $\bar{u}_{ij}$ to replace the Riemann problem solution $u^{RP}_{\Delta x}(t, x)$ and perform numerical integration on the analytical equations (80)-(83). This process leads us to define

$$u_{i,j+1} = \bar{u}_{ij} + \left\{G(\frac{1}{2}(\mathbf{A}_{ij} + \mathbf{A}_{i+1,j}), \hat{u}(\xi - t_j, \bar{u}_{ij}, x))\right\} \Delta t_j. \tag{84}$$

The mass is

$$M_{i,j+1} = M_{r_{min}} + \sum_{k<i} \frac{\kappa}{2} \left(u^0_{\Delta x}(x_{k-}, t_{j+1}) x^2_{k-} \Delta x \right), \tag{85}$$

with

$$u^0_{\Delta x}(x_{k-}, t_{j+1}) = \frac{1}{2}\{u^0_{k-1,j+1} + u^0_{k,j+1}\}, \tag{86}$$

and the metric becomes

$$A_{i,j+1} = 1 - \frac{2M_{i,j+1}}{x_{i-}}, \tag{87}$$

and

$$B_{i,j+1} = B_{r_{min}} e^{\tau}, \tag{88}$$

where

$$\tau = \left\{ \sum_{k<i} \frac{\{A_{k,j+1}\}^{-1} - 1}{x_{k-}} + \frac{\kappa x_{k-}}{A_{k,j+1}} T^{11}_M(u_{\Delta x}(x_{k-}, t_{j+1})) \Delta x \right\}, \tag{89}$$

with

$$u_{\Delta x}(x_{k-}, t_{j+1}) = \frac{1}{2}\{u_{k-1,j+1} + u_{k,j+1}\}. \tag{90}$$

Note that since the metric is staggered relative to the conserved quantities, we use the in between values, like x_{k-} and $u_{\Delta x}(x_{k-}, t_{j+1})$ in the update step. Let $\mathbf{A}_{i,j+1} = (A_{i,j+1}, B_{i,j+1})$ denote the constant value for $\mathbf{A}_{\Delta x}$ on $R_{i,j+1}$. This concludes the update step and completes the definition of the approximate solution $u_{\Delta x}$ and $\mathbf{A}_{\Delta x}$ by induction.

To summarize the method, the locally inertial Godunov method constructs the solution inductively with four major steps: a Riemann problem step, a Godunov step (with time dilation), an ODE step, and an update step. The Riemann problem step is described in equations (72) and (73). Formulas (74)-(76) denote the Godunov step. The ODE step is detailed in (77)-(80). Finally, equations (84)-(90) express the update step.

7 The Riemann Problem Step

In this section we discuss the Riemann problem (RP) step of the locally inertial method. When $\sqrt{AB} = constant$, $p = \sigma\rho$ and we neglect the source terms on the right hand side, equations (13), (14) reduce to

$$u_t + \sqrt{AB} F(u)_x = 0, \tag{91}$$

where

$$u \equiv (u^0, u^1) = \left(\rho[\left(\frac{\sigma + c^2}{c^2} \right) \frac{v^2}{c^2 - v^2} + 1], \;\; \rho(\sigma + c^2) \frac{v}{c^2 - v^2} \right), \tag{92}$$

and

$$F(u) \equiv (F^0, F^1) = \left(\rho(\sigma + c^2) \frac{v}{c^2 - v^2}, \;\; \rho[(\sigma + c^2) \frac{v^2}{c^2 - v^2} + \sigma] \right). \tag{93}$$

The RP is the initial value problem when the initial data $u_0(x)$ consists of two constant states separated by a jump discontinuity at $x = 0$,

$$u_0(x) = \begin{cases} u_L & x < 0 \\ u_R & x > 0. \end{cases} \tag{94}$$

System (91) with (94) define the RP step of the locally inertial method. Except for the extra factor $\sqrt{AB}$, equations (91) agree with the relativistic compressible Euler equations in flat Minkowski spacetime,

$$u_t + F(u)_x = 0, \tag{95}$$

and we will account for the factor $\sqrt{AB}$ by time-dilation. When $\sqrt{AB} = 1$, $p = \sigma\rho$, the RP for the compressible Euler equations was given in closed form in [9]. We summarize the results in the following theorem:

Theorem 7.1. *There exists a solution of the RP for system (95) with an equation of state $p = \sigma\rho$, $0 < \sqrt{\sigma} < c$, as long as u_L and u_R satisfy $\rho_L, \rho_R > 0$ and $-c < v_L, v_R < c$. The solution is given by a 1-wave followed by a 2-wave, satisfies $\rho > 0$, and all speeds are bounded by c. This solution is unique in the class of rarefaction waves and admissible shock waves.*

We now record the exact formulas required in the construction of the RP solutions, c.f. [9]. (These formulas correct typos in [9], specifically in (2.5.73), (2.5.74), (4.2.12), and (4.2.13) recorded in [14].)

To start, the mapping between the conserved variables (u^0, u^1) and the fluid variables (ρ, v), $1-1$ and nonsingular in $\rho > 0$, $|v| < c$, is given by

$$v(u^0, u^1) = \frac{c^2}{2\sigma u^1}\{(\sigma + c^2)u^0 - \sqrt{(\sigma + c^2)^2(u^0)^2 - 4\sigma(u^1)^2}\}. \tag{96}$$

$$\rho(u^0, u^1) = \frac{(c^2 - v^2)u^1}{(\sigma + c^2)v}. \tag{97}$$

The eigenvalues (wave speeds) $\lambda_{1,2} = \lambda_{-,+}$ of DF in (93) are given by

$$\lambda_i = \frac{v \pm \sqrt{\sigma}}{1 \pm \frac{\sqrt{\sigma}v}{c^2}},$$

and the Riemann invariants r and s are

$$r(\rho, v) = \frac{1}{2}\ln\left(\frac{c+v}{c-v}\right) - \sqrt{\frac{K}{2}}\ln(\rho), \tag{98}$$

$$s(\rho, v) = \frac{1}{2}\ln\left(\frac{c+v}{c-v}\right) + \sqrt{\frac{K}{2}}\ln(\rho), \tag{99}$$

where

$$K = \frac{2\sigma c^2}{(\sigma + c^2)^2}. \tag{100}$$

so that (ρ, v) are given by

$$\rho(r,s) = \exp\left\{\frac{s-r}{\sqrt{2K}}\right\}, \tag{101}$$

$$v(r,s) = -\frac{c(1-e^{s+r})}{1+e^{s+r}}. \tag{102}$$

The following formulas are also useful:

$$v(\lambda_1) = \frac{\lambda_1 + \sqrt{\sigma}}{1+\frac{\sqrt{\sigma}\lambda_1}{c^2}}, \qquad v(\lambda_2) = \frac{\lambda_2 - \sqrt{\sigma}}{1-\frac{\sqrt{\sigma}\lambda_2}{c^2}},$$

$$\rho(r,v) = \exp\left\{-\sqrt{\frac{2}{K}}\left(r - \frac{1}{2}\ln\left\{\frac{c+v}{c-v}\right\}\right)\right\}, \tag{103}$$

$$\rho(s,v) = \exp\left\{\sqrt{\frac{2}{K}}\left(s - \frac{1}{2}\ln\left\{\frac{c+v}{c-v}\right\}\right)\right\}. \tag{104}$$

The 1,2-rarefaction curves R_1, R_2 are are the straight lines $s = const.$, $r = const.$ in the plane of Riemann invariants given by,

$$\begin{aligned} U_R &\equiv (r_R(u_R), s_R(u_R)) = (r_R(\rho_R, v_R), s_R(\rho_R, v_R)) \\ U_L &\equiv (r_L(u_L), s_L(u_L)) = (r_L(\rho_L, v_L), s_L(\rho_L, v_L)), \end{aligned} \tag{105}$$

and the 1,2-shock curves S_1, S_2 are given by the following parametrization with respect to β, $0 \le \beta < \infty$:

$$\begin{aligned} \Delta r = r - r_L &= -\frac{1}{2}\ln\{f_+(2K\beta)\} - \sqrt{\frac{K}{2}}\ln\{f_+(\beta)\} \equiv S_1^r(\beta), \\ \Delta s = s - s_L &= -\frac{1}{2}\ln\{f_+(2K\beta)\} + \sqrt{\frac{K}{2}}\ln\{f_+(\beta)\} \equiv S_1^s(\beta), \end{aligned} \tag{106}$$

$$\begin{aligned} \Delta r = r - r_L &= -\frac{1}{2}\ln\{f_+(2K\beta)\} - \sqrt{\frac{K}{2}}\ln\{f_-(\beta)\} \equiv S_2^r(\beta), \\ \Delta s = s - s_L &= -\frac{1}{2}\ln\{f_+(2K\beta)\} + \sqrt{\frac{K}{2}}\ln\{f_-(\beta)\} \equiv S_2^s(\beta), \end{aligned} \tag{107}$$

where

$$f_\mp(\beta) \equiv 1 + \beta\left\{1 \mp \sqrt{1+\frac{2}{\beta}}\right\}, \tag{108}$$

and

$$\beta \equiv \beta(v, v_L) = \frac{(\sigma + c^2)^2}{2\sigma^2}\frac{(v-v_L)^2}{(c^2-v^2)(c^2-v_L^2)}, \tag{109}$$

with shock speeds

$$s_1 = c\sqrt{\frac{f_+(\beta)+\frac{\sigma}{c^2}}{f_+(\beta)+\frac{c^2}{\sigma}}}, \tag{110}$$

$$s_2 = c\sqrt{\frac{f_-(\beta)+\frac{\sigma}{c^2}}{f_-(\beta)+\frac{c^2}{\sigma}}}. \tag{111}$$

The formulas (106), (107) display the so called Nishida property of this system, that i-shock curves based at different points are rigid translations of one another, and 1-shock curves are reflections of 2-shock curves, c.f. [9]. Constructing the Godunov averages requires computing the zero speed middle state of the RP, which is greatly simplified in plane of Riemann invariants by the Nishida property. Vogler's RP algorithm solves for the middle state $u_* \equiv u(t,x) = (\rho_*, v_*)$ by first converting u_L and u_R to Riemann invariants via (98), (99), numerically computing U_M in the rs-plane, then converting U_M back to fluid variables using (101), (102).

8 Time Dilation Between Space Time Cells

When $\sqrt{AB} \neq 1$, the factor can be accounted for in the solution of the RP for (91) in a grid cell by solving the RP for $\sqrt{AB} = 1$, and then rescaling the time in that grid cell, by a factor of $\sqrt{AB}$. The factor $\sqrt{AB}$ has the effect of dilating the physical (geodesic) time in a grid cell relative to the coordinate time, , c.f. Figure 8. Thus, our GR Godunov method has the nice property that it allows for the use of exact RP solutions in each grid cell, and the consequent errors due to neglecting the local curvature are accounted for by simply rescaling the local time relative to coordinate time. The following theorem, based on this, expresses that if the time in a Godunov cell is shortened, the resulting average is an affine combination of the original average and the center state, based on the ratio of the original and new time change.

Theorem 8.1. *Let*

$$\Delta\tilde{t} = \frac{\Delta x}{2\sqrt{AB}} \tag{112}$$

represent the maximum time in a Godunov cell before the CFL condition is violated. If the change in time is shortened from $\Delta\tilde{t}$ to $\Delta t < \Delta\tilde{t}$ in a Godunov cell containing the solution to the RP's $u(t,x)$, the average across that grid cell at time $\Delta\tilde{t}$, $\bar{u}(\Delta\tilde{t})$, and at time Δt, $\bar{u}(\Delta t)$, are related by

$$\bar{u}(\Delta t) = \lambda\bar{u}(\Delta\tilde{t}) + (1-\lambda)u_C \tag{113}$$

where $\lambda = \frac{\Delta t}{\Delta\tilde{t}} < 1$ is the ratio between the two times.

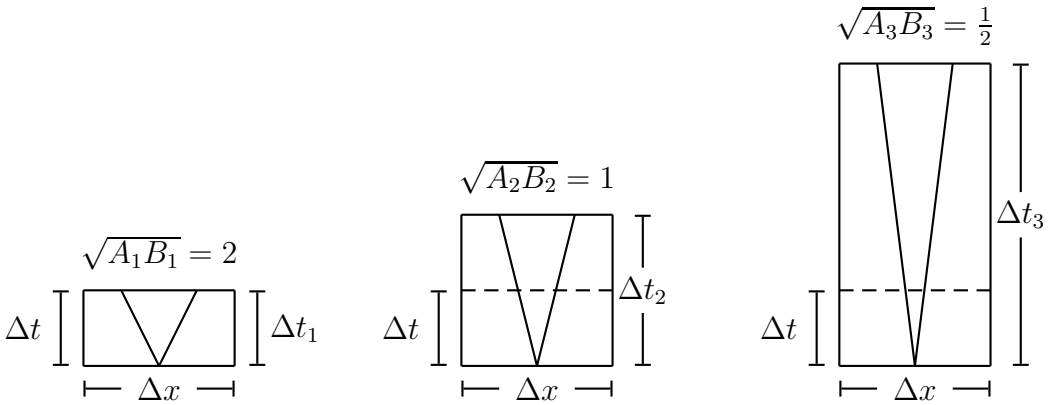

Figure 3: Effects of time dilation

9 Convergence to a Weak Solution

Our main convergence theorem regarding the locally inertial Godunov method with dynamic time dilation is the following.

Theorem 9.1. *Let $u_{\Delta x}(t,x)$ and $\mathbf{A}_{\Delta x}(t,x)$ be the approximate solution generated by the locally inertial Godunov method starting from the initial data $u_{\Delta x}(t_0,x)$ and $\mathbf{A}_{\Delta x}(t_0,x)$ for $t_0 > 0$. Assume these approximate solutions exist up to some time $t_{end} > t_0$ and converge to a solution $(u_{\Delta x}, \mathbf{A}_{\Delta x}) \to (u, \mathbf{A})$ as $\Delta x \to 0$ along with a total variation bound at each time step t_j*

$$T.V._{[r_{min},r_{max}]}\{u_{\Delta x}(t_j,\cdot)\} < V, \tag{114}$$

where $T.V._{[r_{min},r_{max}]}\{u_{\Delta x}(t_j,\cdot)\}$ represents the total variation of the function $u_{\Delta x}(t_j,x)$ on the interval $[r_{min}, r_{max}]$. Assume the total variation is independent of the time step t_j and the mesh length Δx. Then the solution $(u, \mathbf{A})$ is a weak solution to the Einstein equations (9)-(12).

The proof involves demonstrating that the terms in the residual of numerical approximations of the locally inertial Godunov method that do not converge first order in Δx, come back to cancel other terms of the same order, producing only terms first order in Δx. The result implies that only convergence and stability need be numerically verified in order to conclude the limit is a weak solution of the Einstein equations. The proof is omitted. See [16] for details.

10 FRW-TOV Simulation in Forward Time

We now present the results of the forward time simulation of the FRW/TOV matched model. We use the initial profiles (54)-(57) along with the boundary conditions (66)-(71) developed

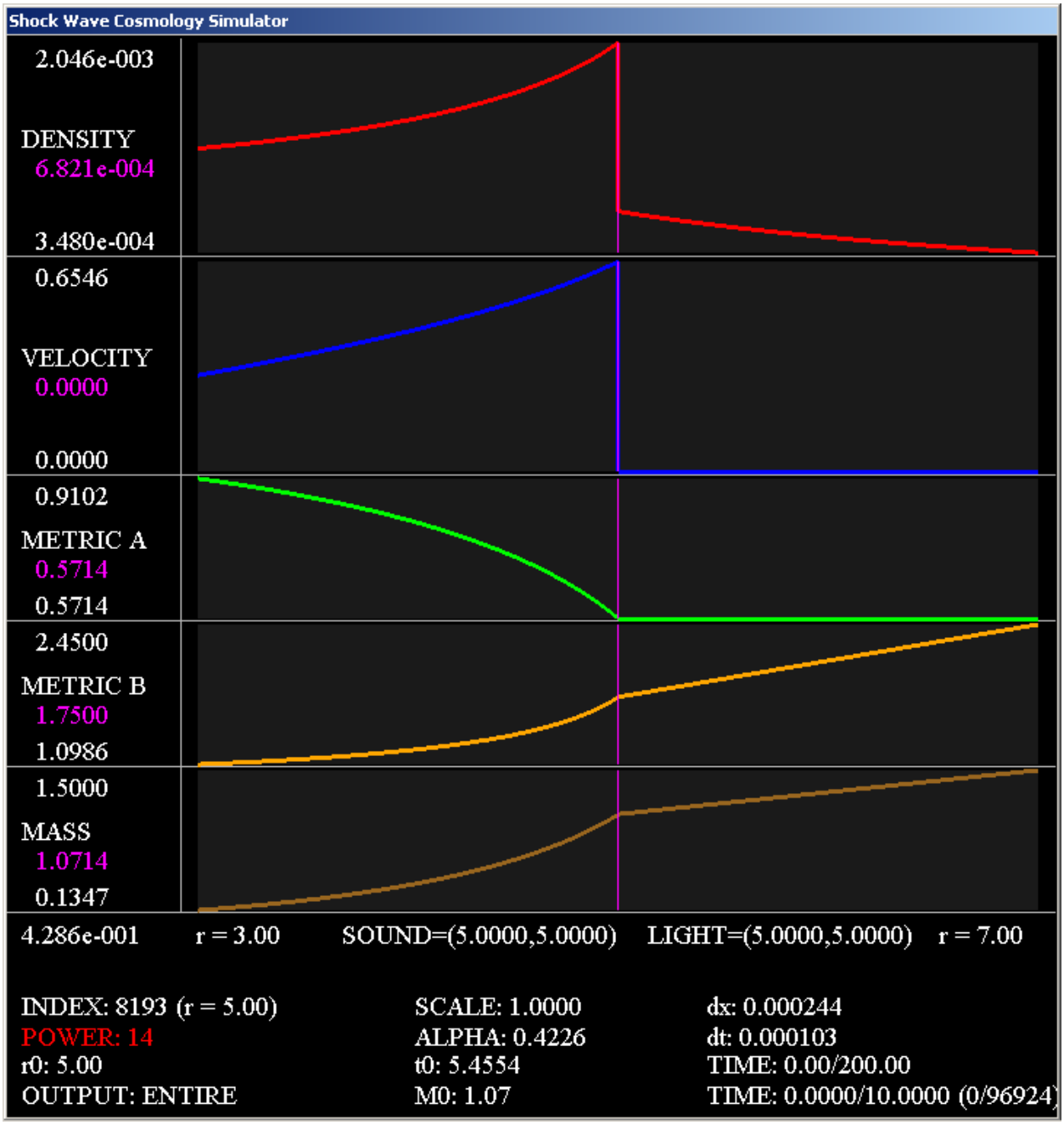

Figure 4: Initial profiles

in the last section to start and run the simulation. Figure 4 shows the initial profiles with these parameters for the fluid variables (ρ_{init}, v_{init}) and the metric $\mathbf{A}_{init}$, along with the mass. By selecting the initial discontinuity at $\bar{r}_0 = 5$, equation (51) gives the initial start time of $\bar{t}_0 = 5.4554$. Note that the discontinuities in the fluid variables jump down from the FRW side to the TOV side. Moreover, the FRW density ρ and the TOV density $\bar{\rho}$ at this discontinuity are related by $\rho = 3\bar{\rho}$.

With these initial profiles, we run the simulation for one unit of time (i.e. $\bar{t}_{end} = \bar{t}_0 + 1$). Figure 5 depicts the evolution of the fluid variables (ρ, v), giving us a frame by frame view for the evolution of the fluid variables across this time frame, evenly distributed from the left frame at $\bar{t}_0$ to the right frame at $\bar{t}_{end}$. After the initial time $\bar{t}_0$, two shock waves form, the stronger shock moving out toward the TOV side and the weaker shock moving in toward the FRW side, creating an intermediate pocket of higher density expanding and interacting with the FRW and TOV metrics on either side. We conclude that the incoming wave, viewed as secondary to the strong outgoing shock wave, for this solution of the Einstein equations is another shock wave, reflected back in.

Next, we focus attention on the resulting solution at the end time, $\bar{t}_{end}$. Figure 6 highlights where the two shock positions are relative to the cone of sound and the cone of light. The cone of light is represented by the white region while the cone of sound, embedded in the cone of light, is represented by the grey region. Note that the edges of the cone of sound align with the shock waves on either side, confirming that the interaction region between the two metrics lies completely within the cone of sound. Since the edges of the cone of sound move at the local sound speed, the explanation here is that the edges of the cone of sound impinge on the shocks like a characteristic, so if one of the edges were to get slightly ahead or behind the shock position, then that edge would get pushed back into the shock like the characteristics close to the shock. Figure 6 also displays the spatial derivatives in the metric components A and B, the green and orange graphs, respectively. The derivatives (A', B'), found using numerical differentiation, have discontinuities aligned with the discontinuities associated with the fluid variables at the edges of the cone of sound. Looking back at Figure 5, it shows the profiles for the metric (A, B) as being continuous, so the metric is Lipschitz continuous, reinforcing the fact that we have a weak solution to the Einstein equations.

Convergence was tested by successive mesh refinements confirming a first order convergence rate. Convergence to FRW and TOV on each side of the interaction region was also confirmed. We also explored simulations for a variety of values of the initial data parameter and came to two conclusions. One is that the resulting solution always has a region of higher density surrounded by two shock waves, a strong shock on the TOV side and a weak shock on the FRW side, and the other is that the shock waves have different speeds, resulting in quantitatively different solutions. We conclude that the initial data set produces a one parameter family of quantitatively different shock wave solutions to the Einstein equations, each representing a point of shock wave interaction emanating from the initial discontinuity in the fluids.

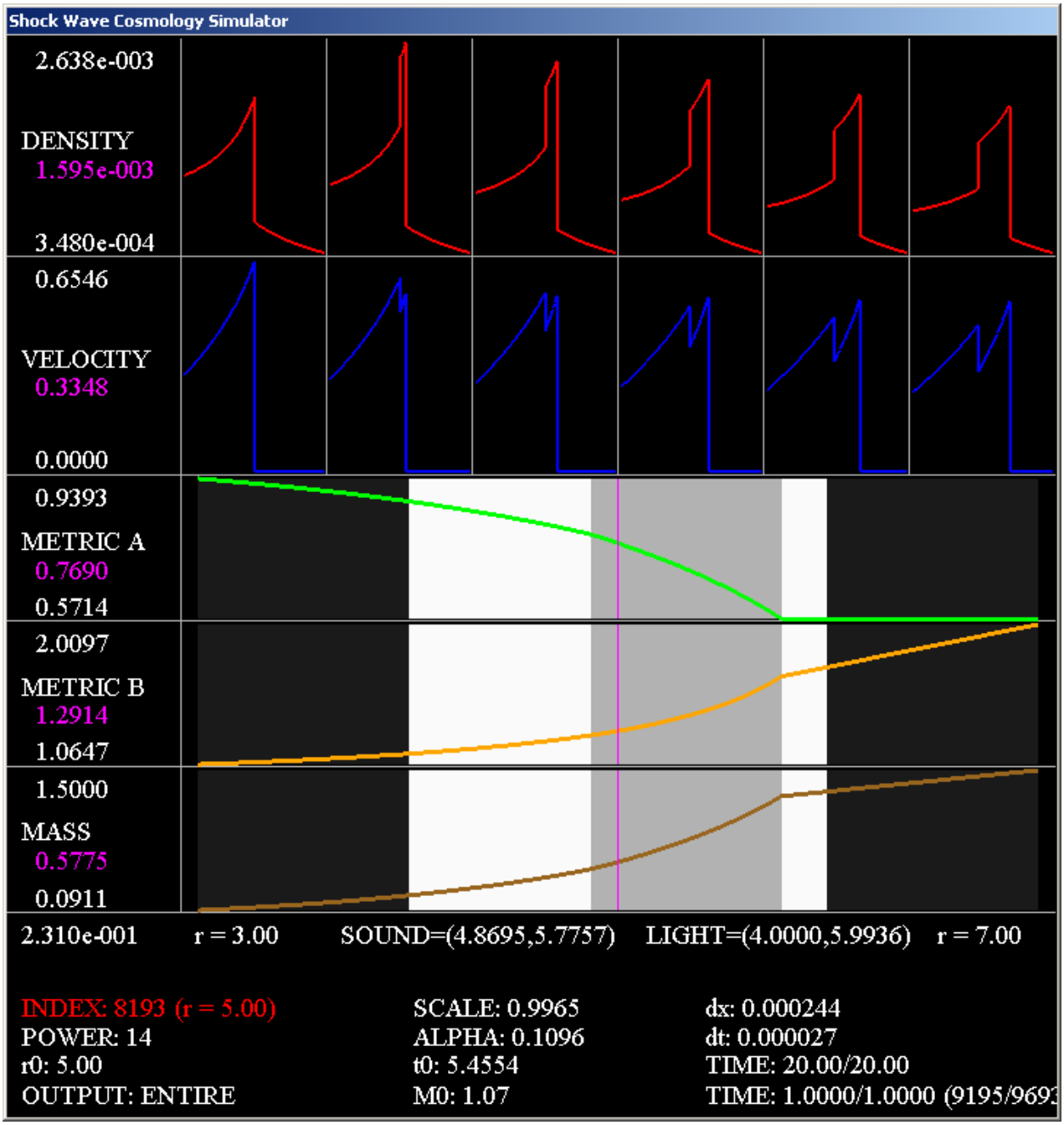

Figure 5: Evolution of the fluid variables during a unit of time

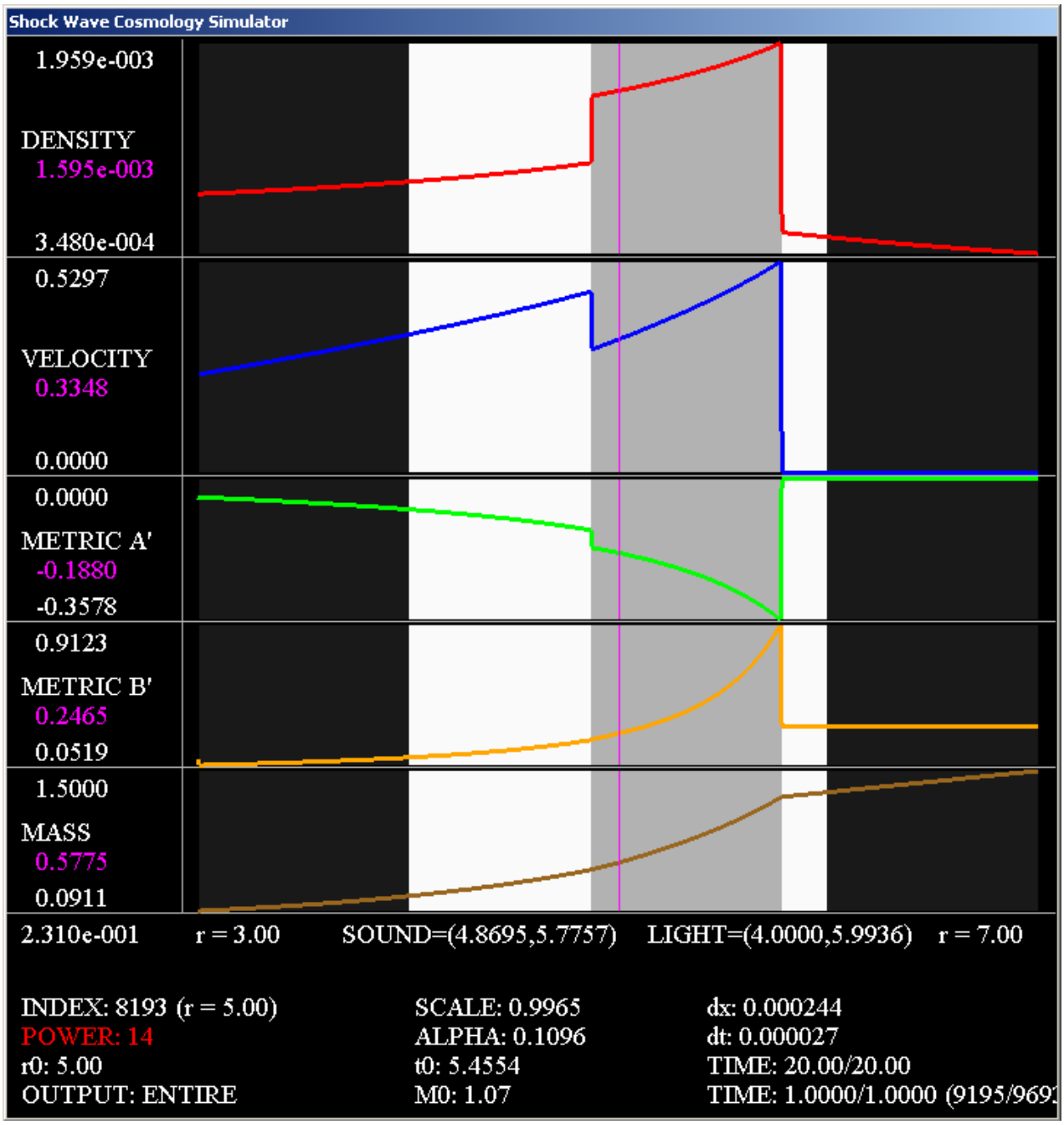

Figure 6: Solution after a unit of time, showing the derivatives of the metric

11 Putting Units into the Simulation

To get a sense of scale in the simulations take the speed of light $c = 2.99 \times 10^5$ km/sec and Newton's constant $\mathcal{G} = 1.47664$ km/$M_\odot$, where $M_\odot = 1.989 \times 10^{30}$ g is the mass of our sun, c.f. [17]. Using this scale, the range of values in our simulations is

$$\begin{aligned}
0.09\ M_\odot < \quad & M & < 1.5\ M_\odot, & (1)\\
4.43\ \text{km} < \quad & \bar{r}_* & < 10.37\ \text{km}, & (2)\\
2.69 \times 10^{-5}\ \text{sec} < \quad & \bar{t}_* & < 3.18 \times 10^{-5}\ \text{sec}, & (3)\\
1.08 \times 10^{-4} M_\odot/\text{km}^3 < \quad & \rho_* & < 5.95 \times 10^{-4} M_\odot/\text{km}^3, & (4)\\
0\ \text{km/sec} < \quad & v & < 1.59 \times 10^5\ \text{km/sec}. & (5)
\end{aligned}$$

In this case our simulations correspond to a mass of about 1.4 times our sun across a distance of about 5.94 kilometers for a time interval of about 4.9 microseconds. The average density of the sun is $7.04 \times 10^{-19} M_\odot/\text{km}^3$, so our simulated densities are about 1.53×10^{14} times greater than the average density of the sun, and matter is moving at speeds up to 1.59×10^5 km/sec.

On a galactic scale, set one unit of mass equal to the mass of the Milky Way, about $1.8 \times 10^{11}\ M_\odot$. On this scale the simulated values become

$$\begin{aligned}
1.62 \times 10^{10}\ M_\odot < \quad & M & < 2.7 \times 10^{11}\ M_\odot, & (6)\\
0.084\ \text{light-years} < \quad & \bar{r}_* & < 0.2\ \text{light-years}, & (7)\\
56\ \text{days} < \quad & \bar{t}_* & < 66\ \text{days}, & (8)\\
1.94 \times 10^7 M_\odot/\text{km}^3 < \quad & \rho_* & < 1.07 \times 10^8 M_\odot/\text{km}^3, & (9)\\
0\ \text{km/sec} < \quad & v & < 1.59 \times 10^5\ \text{km/sec}. & (10)
\end{aligned}$$

Therefore, on the galactic scale, our simulation corresponds to a mass equivalent to about 1.4 times our Milky Way across a distance of about 0.12 light-years in a time interval of about 10 days.

12 Conclusion

We have recorded the basic formulas used to construct the locally inertial Godunov method incorporating time dilation, and the initial data we tested it on (shown in Figure 4). Figure 5 provided snapshots of our simulation of a point of shock wave interaction. The solution resolves a solution of the Einstein equations in SSC coordinates in which two radial shock waves emerge from a point of interaction, generating a strong outgoing wave and a weak incoming wave, enveloping a region of higher density created by the interaction. Changing the parameter $\bar{r}$ produces quantitatively different solutions that are qualitatively the same. The simulated solution only solves the Einstein equations weakly because of discontinuities in the derivatives of the metric, as shown in Figure 6. We demonstrate that the region of

interaction lies within the cone of sound by recording convergence between the position of the shock waves and the edges of the cone of sound, (c.f. [16]). The simulation imposes boundary data on the FRW side of a region of interaction, and recovers the TOV metric on the other side by integrating across the interaction region. The numerical convergence of the FRW and TOV metrics in the non-interaction regions, is recorded in [16]. A proof of the convergence of the residual tailored to this problem is recorded in Theorem 9.1. The theorem reduces the problem of proving the simulated solution solves the Einstein equations, to the much simpler problem of demonstrating numerical convergence alone. The simulation resolves the "secondary wave" in [11] as a reflected shock wave. In summary, this is a successful demonstration of numerical convergence at a point of shock wave interaction, in a GR framework tailored for a definitive test of numerical convergence, in a coordinate system where the gravitational metric appears singular at shocks. A recent proof by Rientes, (to appear with second author), shows that such points of shock wave interaction are indeed a new kind of singularity in general relativity in the sense that the gravitational metric tensor cannot be smoothed to $C^{1,1}$ at points of shock wave interaction having the structure simulated here.

References

[1] J. Glimm, *Solutions in the large for nonlinear hyperbolic systems of equations*, Comm. Pure Appl. Math., **18**, 697-715 (1965).

[2] J. Groah and B. Temple, *Shock-wave solutions of the Einstein equations: Existence and consistency by a locally inertial Glimm Scheme*, Memoirs of the AMS, Vol. 172, No. 813, November 2004.

[3] S.W. Hawking and G.F.R. Ellis, *The Large Scale Structure of Spacetime*, Cambridge University Press, 1973.

[4] P.D. Lax, *Hyperbolic systems of conservation laws, II*, Comm. Pure Appl. Math., **10**, 537–566 (1957).

[5] W. Israel, "Singular hypersrfaces and thin shells in general relativity", Il Nuovo Cimento, Vol. XLIV B, N. 1, pp. 1-14 (1966).

[6] D. Nelson and M. Choptuik, , *Ultra-relativistic fluid dynamics*, arXiv:-qc/9904052v1 20 Apr 1999.

[7] T. Nishida, *Global solution for an initial boundary value problem of a quasilinear hyperbolic system*, Proc. Jap. Acad., **44**, (1968), pp. 642-646.

[8] J. Smoller, *Shock Waves and Reaction Diffusion Equations*, Springer Verlag, 1983.

[9] J. Smoller and B. Temple *Global solutions of the relativistic Euler equations*, Comm. Math. Phys., **157**, 67-99 (1993).

[10] J. Smoller and B. Temple, *General relativistic shock–waves that extend the Oppenheimer–Snyder model*, Arch. Rat. Mech. Anal. **138**, (1997), pp. 239-277.

[11] J. Smoller and B. Temple, *Astrophysical shock wave solutions of the Einstein equations*, Phys. Rev. D, **51**, no. 6, (2733–2743)

[12] J. Smoller and B. Temple, *Solutions of the Oppenheimer-Volkoff equations inside 9/8'ths of the Schwarzschild radius*, with J. Smoller, Commun. Math. Phys. **184**, (1997), 597-617.

[13] J. Smoller and B. Temple, *Cosmology, black holes, and shock waves beyond the Hubble length*, Meth. Appl. Anal., **11**, 77-132 (2004).

[14] J. Groah, J. Smoller and B. Temple, *Shock Wave Interactions in General Relativity*, Springer Monographs, Springer 2007.

[15] B. Temple and J. Smoller, *Expanding wave solutions of the Einstein equations that induce an anomalous acceleration into the Standard Model of Cosmology*, Proc. Nat. Acad. Sci., August 25, 2009, Vol. 106, no. 34, (14213-14218).

[16] Z. Vogler, *The Numerical Simulation of General Relativistic Shock Waves by a Locally Inertial Godunov Method Featuring Dynamic Time Dilation*, Doctoral Dissertaion, UC-Davis, March 2010.

[17] S. Weinberg, *Gravitation and Cosmology: Principles and Applications of the General Theory of Relativity*, John Wiley & Sons, New York, 1972.